

## Atmosphere–Ocean Modeling Exploiting Fluid Isomorphisms

JOHN MARSHALL, ALISTAIR ADCROFT, JEAN-MICHEL CAMPIN, AND CHRIS HILL

*Program in Atmospheres, Oceans and Climate, Department of Earth, Atmospheric and Planetary Sciences, Massachusetts Institute of Technology, Cambridge, Massachusetts*

ANDY WHITE

*Met Office, Bracknell, United Kingdom*

(Manuscript received 3 February 2003, in final form 27 May 2004)

### ABSTRACT

Mathematical isomorphisms between the hydrostatic equations that govern the evolution of a compressible atmosphere and an incompressible ocean are described and exploited to guide the design of a hydrodynamical kernel for simulation of either fluid.

### 1. Introduction

The large-scale circulation of the atmosphere and ocean are governed by equations and boundary conditions that are similar to one another because the underlying fluid dynamics are the same. Yet the development of numerical models of the atmosphere and ocean has occurred almost independently. There has been delayed exchange of ideas developed in one application for use in the other. The reasons for this lie largely, we believe, in the sociology of the two disciplines. Atmospheric and oceanic models are developed by different groups of scientists, with different goals and levels of support and who often do not communicate with one another. But the increasing importance of and challenges posed by coupled climate modeling has meant that the need for collaboration is urgent.

Here we report on an approach to coupled climate modeling in which the same hydrodynamical algorithm is used to simulate both the atmosphere and ocean by exploiting the well-known<sup>1</sup> isomorphism between the equations that govern the respective fluids. Detailed treatment and exploitation of the isomorphism is rare, however, and is the goal of this paper. From one hydrodynamical kernel, separate atmospheric and oceanic models are rendered by use of appropriate physics

---

<sup>1</sup> Eliassen (1949), for example, says of the hydrodynamic equations in  $p$  coordinates “the equations prove simpler than in the usual form; and some of them become formally identical to the equations for a homogeneous and incompressible fluid”.

---

*Corresponding author address:* Dr. John Marshall, 77 Massachusetts Avenue, Room 54-1526, Cambridge, MA 02139-4307.  
E-mail: marshall@gulf.mit.edu

“overlaid” on the dynamics, as illustrated schematically in Fig. 1. Although the hydrodynamical kernel described has been developed with the express purpose of using it for simulation of either fluid, existing atmospheric/oceanic models could be “converted” from one to the other.

In section 2 we discuss the theoretical underpinning of our approach. In section 3 we describe the formulation and implementation of the ideas in the MIT hydrodynamical kernel, Marshall et al. (1997a,b). In particular we discuss how one can use a normalized pressure coordinate related to eta coordinates (Mesinger et al. 1988) to represent the lower boundary condition of the atmospheric model. In section 4 we present illustrations of the kernel in action in studies of both fluids. In section 5 we summarize and conclude.

### 2. Atmosphere–ocean fluid isomorphisms

We begin by simply stating the equations of motion and boundary conditions that govern the large-scale atmosphere and ocean in pressure and height coordinates, respectively. We exploit the well-known fact that these equations are isomorphic: a simple mapping between coordinates and state variables renders complementary equations and boundary conditions. For the purposes of designing a single hydrodynamical kernel to model both atmosphere and ocean, we then go on to write the equations of motion in terms of a generic vertical coordinate,  $r$ .

#### *a. Pressure coordinate equations for the atmosphere*

The equations representing the evolution of a compressible, hydrostatic atmosphere in pressure coordinates are (see, e.g., Haltiner and Williams 1980):

$$\frac{D}{Dt} \mathbf{v}_h + f \mathbf{k} \times \mathbf{v}_h + \nabla_p \Phi = \mathcal{F} \tag{1}$$

$$\frac{\partial \Phi}{\partial p} + \alpha = 0 \tag{2}$$

$$\nabla_p \cdot \mathbf{v}_h + \frac{\partial \omega}{\partial p} = 0 \tag{3}$$

$$\alpha = \alpha(\theta, p) = \frac{\partial \Pi}{\partial p} \theta \tag{4}$$

$$\frac{D}{Dt} \theta = \frac{Q_\theta}{\Pi} \tag{5}$$

$$\frac{D}{Dt} q = Q_q, \tag{6}$$

where  $\mathbf{v}_h = (u, v, 0)$  is the horizontal component of velocity,  $\omega = (D/Dt)p$  is the vertical velocity in pressure coordinates,  $f$  is the Coriolis parameter,  $\mathbf{k}$  is a unit vector in the vertical,  $\Phi = gz$  is the geopotential,  $\alpha$  is the specific volume,  $T$  is the temperature,  $\theta = c_p T / \Pi$  is the potential temperature,  $\Pi = c_p (p/p_0)^\kappa$  is the Exner function, and  $q$  is specific humidity. Here  $c_p$  is the specific heat at constant pressure,  $\kappa = R/c_p$  with  $R$  the gas constant and  $D/Dt = \partial/\partial t + \mathbf{v}_h \cdot \nabla_p + \omega(\partial/\partial p)$  is the total derivative in pressure coordinates.

The terms  $\mathcal{F}$ ,  $Q_\theta$ , and  $Q_q$  represent sources and sinks of momentum, heat, and moisture, respectively. They must be parameterized.

The total energy equation can be formed by taking the dot product of  $\mathbf{v}_h$  with (1), adding  $\omega$  times (2) and  $\Pi$  times (5) to give

$$\frac{D}{Dt} \left( \frac{1}{2} |\mathbf{v}_h|^2 + \Phi + \Pi \theta \right) = \mathbf{v}_h \cdot \mathcal{F} + Q_\theta + \partial_t \Phi, \tag{7}$$

where  $\Pi \theta = c_p T$  is the enthalpy.<sup>2</sup>

ATMOSPHERIC BOUNDARY CONDITIONS

The boundary conditions at the top and bottom of the atmosphere, shown schematically in Fig. 2, are<sup>3</sup>

<sup>2</sup> To derive Eq. (7) we made use of the following relations:

$$\begin{aligned} \Pi \frac{D}{Dt} \theta &= \frac{D}{Dt} (\Pi \theta) - \theta \frac{D}{Dt} \Pi \\ &= \frac{D}{Dt} (\Pi \theta) - \theta \partial_p \Pi \frac{D}{Dt} p = \frac{D}{Dt} (\Pi \theta) - \alpha \omega. \end{aligned}$$

<sup>3</sup> Equation (8) is the exact upper boundary condition but Lindzen et al. (1968) have shown that when this is employed in a model with discrete levels, there may be false reflection of energy that can have a deleterious effect on lower levels. This problem can be ameliorated by incorporating a damping process (a ‘‘sponge layer’’) in the uppermost levels of the model—see discussion in Haltiner and Williams (1980).

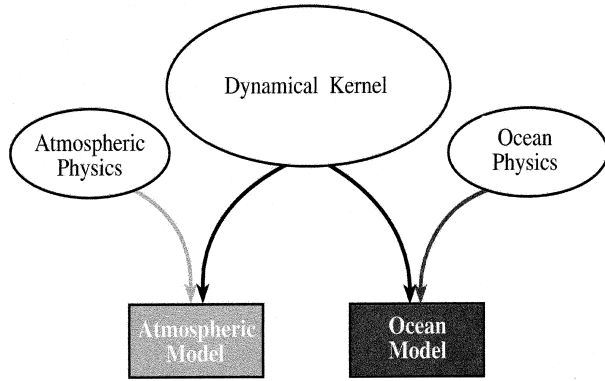


FIG. 1. A single dynamical kernel is used to drive forward both oceanic or atmospheric models.

$$\omega = \begin{cases} 0 & \text{at } p = 0 \text{ (top of the atmosphere),} \\ \frac{Dp_s}{Dt} & \text{at } p = p_s(x, y, t) \\ & \text{(bottom of the atmosphere),} \end{cases} \tag{8}$$

where  $p_s$  is the surface pressure. The boundary condition used on integration of the hydrostatic equation (2) is

$$\Phi = \Phi_s = gH \quad \text{at } p = p_s(x, y, t),$$

where  $H$  is the height of the mountains at the lower boundary.

The surface pressure evolves according to

$$\frac{\partial}{\partial t} p_s + \nabla \cdot (p_s \widehat{\mathbf{v}}_h) = 0, \tag{9}$$

where

$$\widehat{\mathbf{v}}_h = \frac{1}{p_s} \int_0^{p_s} \mathbf{v}_h dp$$

is the  $p$ -averaged horizontal wind.

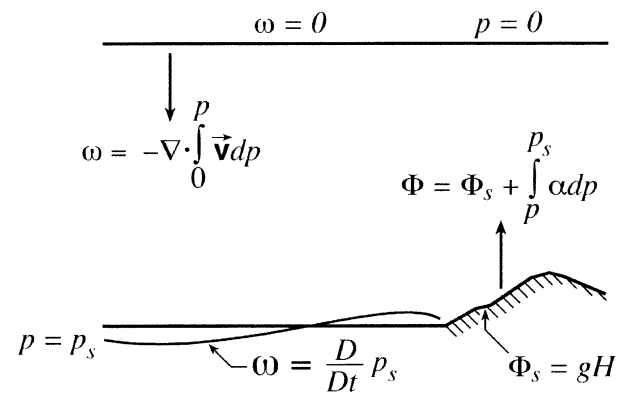


FIG. 2. The vertical structure of the atmospheric model. The hydrostatic equation is integrated up from the lower boundary to yield geopotential height, the continuity equation down from the upper boundary to yield vertical velocity.

*b. Z-coordinate equations for the ocean*

The hydrostatic equations of motion for an incompressible, Boussinesq ocean in height coordinates are

$$\frac{D}{Dt} \mathbf{v}_h + f \mathbf{k} \times \mathbf{v}_h + \nabla_z \left( \frac{p}{\rho_o} \right) = \mathcal{F} \tag{10}$$

$$\frac{\partial}{\partial z} \left( \frac{p}{\rho_o} \right) + g \frac{\rho}{\rho_o} = 0 \tag{11}$$

$$\nabla_z \cdot \mathbf{v}_h + \partial_z w = 0 \tag{12}$$

$$\rho = \rho(\theta, S, p) \tag{13}$$

$$\frac{D}{Dt} \theta = Q_\theta \tag{14}$$

$$\frac{D}{Dt} S = Q_s, \tag{15}$$

where  $\mathbf{v}_h = (u, v, 0)$  is the horizontal component of velocity,  $w = (D/Dt)z$  is the vertical velocity,  $p$  is the pressure,  $\rho(\theta, S, p)$  is the density,  $\rho_o$  is a constant reference density,  $\theta$  is the potential temperature,  $S$  is the salinity, and  $D/Dt = \partial/\partial t + \mathbf{v}_h \cdot \nabla_z + w(\partial/\partial z)$  is the total derivative in  $z$  coordinates.

The terms  $\mathcal{F}$ ,  $Q_\theta$ , and  $Q_s$  represent sources and sinks of momentum, heat, and salinity, respectively.

An equation for kinetic energy + potential energy can be formed by taking the dot product of  $\rho_o \mathbf{v}_h$  with Eq. (10), adding  $\rho_o w$  times Eq. (11) to give

$$\frac{D}{Dt} \left( \rho_o \frac{1}{2} |\mathbf{v}_h|^2 + g \rho z \right) + \nabla_3 \cdot (\mathbf{v}_3 p) = \mathbf{v}_h \cdot \mathcal{F} + g z \frac{D}{Dt} \rho. \tag{16}$$

The source term in Eq. (16) involving  $(D/Dt)\rho = \partial\rho/\partial\theta|_S Q_\theta + \partial\rho/\partial S|_\theta Q_s + \partial\rho/\partial p|_{S,\theta} (D/Dt)p$  is complicated by the nonlinear equation of state. Note that the Boussinesq model approximates total energy by internal energy [whose evolution is governed by Eq. (14)]: the kinetic energy and potential energy, Eq. (16), appear at higher order; independently of the internal energy.

OCEANIC BOUNDARY CONDITIONS

The boundary conditions at the bottom and top of the ocean, shown schematically in Fig. 3, are

$$w = \begin{cases} -\mathbf{v}_h \cdot \nabla H & \text{at } z = -H \text{ (ocean bottom),} \\ \frac{D\eta}{Dt} = -(P - E) & \text{at } z = \eta \text{ (ocean surface),} \end{cases} \tag{17}$$

where  $P - E$  is precipitation minus evaporation.

The boundary condition used in integration of the hydrostatic equation is

$$p = p_s \text{ at } z = \eta,$$

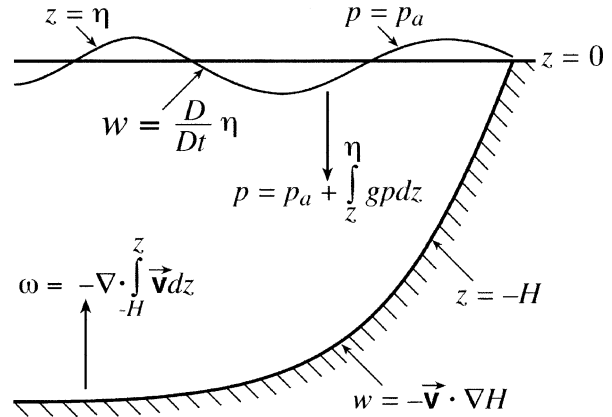


FIG. 3. The vertical structure of the ocean model. The hydrostatic equation is integrated down from the surface to yield the pressure field; the continuity equation up from the bottom to yield the vertical velocity.

where  $p_s$  is the pressure exerted by the atmosphere at the ocean's surface.

The surface elevation evolves according to

$$\frac{\partial}{\partial t} \eta + \nabla \cdot [(H + \eta) \widehat{\mathbf{v}}_h] = P - E, \tag{18}$$

where

$$\widehat{\mathbf{v}}_h = \frac{1}{(H + \eta)} \int_{-H}^{\eta} \mathbf{v}_h dz$$

is the depth-averaged horizontal velocity.

*c. The isomorphism*

If we simply replace the variables and coordinates in sections 2a and 2b—set out in Eqs. (1)–(6) and Eqs. (10)–(15)—thus

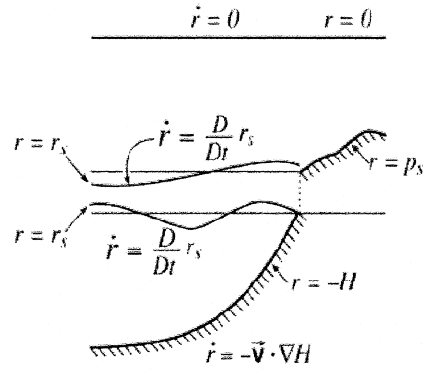
ocean	↔	atmos	iso
$z$	↔	$p$	$r$
$w$	↔	$\omega$	$\dot{r}$
$\frac{p}{\rho_o}$	↔	$\Phi$	$\phi$
$-g \frac{\rho}{\rho_o}$	↔	$-\alpha$	$b$
$\theta$	↔	$\theta$	$\theta$
$S$	↔	$q$	$s$
$\eta$	↔	$p_s$	$r'_s$
$P - E$	↔	0	$P_r$ ,

then we see that the equation sets representing atmospheric and oceanic motion are isomorphic—see Fig. 4.

It is important to note that the boundary conditions—Eqs. (8) and (17)—and the equations governing the evolution of the “free surface” in the respective fluids—Eqs. (9) and (18)—are also exactly isomorphic.

The equations in ‘r’ coordinates

$$\begin{aligned} \frac{D\vec{v}_h}{Dt} + f\mathbf{k} \times \vec{v}_h + \nabla_r \phi &= \vec{\mathcal{F}} \\ \frac{\partial \phi}{\partial r} - b &= 0 \\ \nabla_r \cdot \vec{v}_h + \frac{\partial \dot{r}}{\partial r} &= 0 \\ b &= b(\theta, s, r) \\ \frac{D\theta}{Dt} &= Q_\theta \\ \frac{Ds}{Dt} &= Q_s \end{aligned}$$



Boundary conditions

$$\frac{\partial r_s}{\partial t} + \nabla_h \cdot \int_{p_{fixed}}^{p_s} \vec{v}_h dr = P_r$$

$$\dot{r} = -\vec{v} \cdot \nabla R_{fixed} \text{ at } r = R_{fixed}$$

$$\dot{r} = \frac{Dr_s}{Dt} - P_r \text{ at } r = R_s$$

<i>ocean</i>	← r →	<i>atmos</i>
<i>z</i>		<i>p</i>
<i>w</i>		<i>ω</i>
$\frac{p}{\rho_0}$		$\Phi$
$-\frac{p}{\rho_0}$		$-\alpha$
$\theta$		$\theta$
<i>S</i>		<i>q</i>
$\eta$		$p'_s$
<i>P</i> – <i>E</i>		0

FIG. 4. The atmosphere and ocean rendered in terms of the ‘r’ coordinate.

d. General purpose equations in ‘r’ coordinates

To render atmosphere and ocean models from one dynamical core we exploit the aforementioned ‘‘isomorphisms’’ between equation sets and boundary conditions that govern the hydrostatic evolution of the respective fluids. One system of hydrodynamical equations is written down and encoded in a generic coordinate ‘‘r.’’ The model variables have different interpretations depending on whether the atmosphere or ocean is being studied. Thus, for example, the vertical coordinate of our hydrodynamical kernel, ‘r’, is interpreted as pressure, *p*, if we are modeling the atmosphere and height, *z*, if we are modeling the ocean—(see Fig. 4 and section 2c).

The state of the fluid at any time is characterized by the distribution of velocity *v*, active tracers  $\theta$  and *s*, a ‘‘geopotential’’  $\phi$ , and buoyancy  $b = b(\theta, s, p)$  which may depend on  $\theta, s$ , and *p*. The equations that govern

the evolution of these fields<sup>4</sup> are, written in terms of a generic vertical coordinate, *r*:

$$\frac{D\mathbf{v}_h}{Dt} + f\mathbf{k} \times \mathbf{v}_h + \nabla_r \phi = \mathcal{F} \tag{19}$$

$$\frac{\partial \phi}{\partial r} - b = 0 \tag{20}$$

$$\nabla_r \cdot \mathbf{v}_h + \frac{\partial \dot{r}}{\partial r} = 0 \tag{21}$$

$$b = b(\theta, s, r) \tag{22}$$

$$\frac{D\theta}{Dt} = Q_\theta \tag{23}$$

$$\frac{Ds}{Dt} = Q_s \tag{24}$$

<sup>4</sup>Note that we make the hydrostatic approximation— isomorphic nonhydrostatic forms are not discussed here.

Here,  $r$  is the vertical coordinate,

$$\frac{D}{Dt} = \frac{\partial}{\partial t} + \mathbf{v}_h \cdot \nabla + \dot{r} \frac{\partial}{\partial r} \quad (25)$$

is the total derivative,

$$\nabla = \nabla_h + \mathbf{k} \frac{\partial}{\partial r} \text{ is the "grad" operator}$$

with  $\nabla_h$  operating in the horizontal on surfaces of constant  $r$  and  $\mathbf{k}(\partial/\partial r)$  operating in the vertical, where  $\mathbf{k}$  is a unit vector in the vertical,  $t$  is time,  $\mathbf{v} = (u, v, \dot{r}) = (\mathbf{v}_h, \dot{r})$  is the velocity,  $\phi$  is the "pressure" or geopotential,  $f$  is the Coriolis parameter,  $b$  is the "buoyancy,"  $\theta$  is potential temperature,  $s$  is specific humidity in the atmosphere, salinity in the ocean,  $\mathcal{F}$  represents forcing and dissipation of  $\mathbf{v}$ ,  $Q_\theta$  represents forcing and dissipation of  $\theta$ , and  $Q_s$  represents forcing and dissipation of  $s$ .

The fields  $\mathcal{F}$ ,  $Q_\theta$ , and  $Q_s$  are provided by physical parameterizations of subgrid-scale turbulent fluxes in the atmosphere and ocean. The simple parameterizations used to test our modeling approach are described in the appendix.

1) KINEMATIC BOUNDARY CONDITIONS

In discussion of the vertical axis of the model it is useful to distinguish between boundaries which are fixed and boundaries which are moving in our  $r$  coordinate—see Fig. 4. In the atmosphere where  $r \rightarrow p$  and increases downward, the upper boundary ( $r = 0$ ) is fixed and the lower boundary ( $r = p_s$ , the surface pressure) moves. In the ocean where  $r \rightarrow z$  and increases upward, the lower boundary ( $r = -H$ , the bathymetry) is fixed and the upper boundary ( $r_s = \eta$ , the height of the free surface about its resting position) moves.

At bounding  $r$  surfaces we set (see Fig. 4):

$$\dot{r} = \begin{cases} -\mathbf{v} \cdot \nabla R_{\text{fixed}} & \text{at } r = R_{\text{fixed}} \\ \frac{Dr_s}{Dt} - P_r & \text{at } r = R_s, \end{cases} \quad (26)$$

where

$$R_{\text{fixed}} = \begin{cases} -H & \text{at the bottom of the ocean} \\ 0 & \text{at the top of the atmosphere} \end{cases}$$

defines the position of the fixed bounding coordinate surface and

$$R_s = R_o + r_s \quad (27)$$

defines the position of the moving bounding coordinate surface where

$$R_o = \begin{cases} 0 & \text{at the surface of the ocean} \\ R_o(x, y) = p_s^o(x, y) & \text{at the ground} \end{cases}$$

is the reference position of the moving boundary and

$$r_s = \begin{cases} \eta & \text{at the surface of the ocean} \\ p_s' & \text{at the ground.} \end{cases}$$

are the deviations from the reference.

In Eq. (26),

$$P_r = \begin{cases} P - E & \text{at the surface of the ocean} \\ 0 & \text{in the atmosphere} \end{cases}$$

is the volume flux through  $r_s$ .

Note that  $R_s$  is the "r-value" of the moving bounding coordinate surface—that is, the upper surface of the ocean, the bottom surface in the atmosphere. If the fluid is at rest then this bounding coordinate takes on the value  $R_o(x, y)$ ; when the fluid is moving the bounding coordinate moves about this reference by an amount  $r_s$ . Thus in the ocean,  $R_o = 0$ ;  $r_s = \eta$  is the height of the free surface about its resting height,  $R_o$ , chosen to be zero; in the atmosphere,  $R_o = p_s^o(x, y)$ ;  $r_s = p_s'$ , the fluctuation of the surface pressure about its reference value,  $p_s^o(x, y)$ .

At lateral boundaries, we suppose that there is no normal flow and impose

$$\mathbf{v} \cdot \mathbf{n} = 0,$$

where  $\mathbf{n}$  is the normal to a solid boundary.

2) ISOMORPHIC INTERPRETATION

(i) Atmosphere: 'r = p'

In the atmosphere—see Figs. 2 and 4—we interpret

$$r = p \quad \text{as the pressure} \quad (28)$$

$$\dot{r} = \frac{Dp}{Dt} = \omega \quad \text{as the vertical velocity in } p \text{ coordinates} \quad (29)$$

$$\phi = \Phi = gz \quad \text{as the geopotential height} \quad (30)$$

$$b = -\alpha = -\frac{\partial \Pi}{\partial p} \theta \quad \text{as the buoyancy} \quad (31)$$

$$\theta = T \left( \frac{p_o}{p} \right)^\kappa \quad \text{as potential temperature} \quad (32)$$

$$s = q, \quad \text{as the specific humidity,} \quad (33)$$

where  $T$  is absolute temperature,  $p$  is the pressure, and  $z$  is the height of the pressure surface.

At the top of the atmosphere (which is "fixed" in our  $r$  coordinate):

$$R_{\text{fixed}} = p_{\text{top}} = 0.$$

In an atmosphere at rest the pressure at the top of the mountains is given by

$$R_s = R_o(x, y) = p_s^o(x, y)$$

and the geopotential height of the mountains is

$$\phi = gH_{\text{topo}} = \int_{p_s^o}^{1000 \text{ hPa}} \alpha_{\text{ref}} dp \quad (34)$$

assuming mean sea level pressure is 1000 hPa.

The boundary conditions at the top and bottom are given by

$$\dot{r} = \begin{cases} 0 & \text{at } r = p_{\text{top}} = 0 \text{ (top of the atmosphere),} \\ \frac{Dr_s}{Dt}; & \text{at } r = R_s = p_s(x, y) \\ \frac{Dz}{Dt} & \text{(bottom of the atmosphere),} \end{cases}$$

where  $p_s = p_s^o + p_s'$  is the surface pressure and (because there is no term analogous to  $P - E$  arising in the atmosphere)  $P_r = 0$ .

With the interpretation of variables set out in Eqs. (28)–(33), Eqs. (19)–(27) then yield the set of atmospheric equations and boundary conditions in  $p$  coordinates, written out in section 2a.

(ii) *Ocean*: ‘ $r = z$ ’

In the ocean—see Figs. 3 and 4—we interpret

$$r = z \quad \text{as the height} \quad (35)$$

$$\dot{r} = \frac{Dz}{Dt} = w \quad \text{as the vertical velocity} \quad (36)$$

$$\phi = \frac{P}{\rho_o} \quad \text{as the pressure} \quad (37)$$

$$b = -g \frac{\rho(\theta, S, r)}{\rho_o} \quad \text{as the buoyancy,} \quad (38)$$

where  $\rho_o$  is a fixed reference density of water and  $g$  is the acceleration due to gravity.

At the bottom of the ocean

$$R_{\text{fixed}}(x, y) = -H(x, y)$$

At the surface of the ocean

$$R_s = \eta,$$

where  $\eta$  is the elevation of the free surface because  $R_o = 0$ .

The boundary conditions at the top and bottom of the ocean are

$$\dot{r} = -\mathbf{v} \cdot \nabla R_{\text{fixed}} \quad \text{with}$$

$$R_{\text{fixed}} = -H \text{ (ocean bottom),}$$

$$\dot{r} = \frac{Dr_s}{Dt} - P_r \quad \text{at } r = \eta \text{ (ocean surface) with}$$

$$P_r = P - E.$$

With the interpretation of variables set out in Eqs. (35)–(38), Eqs. (19)–(27) yield a consistent set of ocean equations which are written out in  $z$  coordinates in section 2b.

### 3. A hydrodynamical kernel for simulation of the circulation of the atmosphere and ocean

The model we use to step forward Eqs. (19) to (27)—the MITgcm—employs the “pressure method” comprising prognostic steps for velocity and tracer fields and a diagnostic step to find the pressure field required to maintain three-dimensionally nondivergent flow from one time step to another. Details of the numerical method can be found in Marshall et al. (1997a,b). Briefly, we proceed by dividing the total potential into two parts, a surface part  $\phi_s(x, y)$ , and a hydrostatic part  $\phi_{\text{hyd}}(x, y, r)$ , and writing the momentum equation in the form

$$\frac{\partial}{\partial t} \mathbf{v}_h + \nabla_r \phi_s + \nabla_r \phi_{\text{hyd}} = \mathbf{G}_v, \quad (39)$$

where  $\mathbf{G}_v$  represent advective, Coriolis, and stress terms.

Of interest here, in the context of fluid isomorphisms, is the diagnostic step used to obtain hydrostatic and “surface” pressure fields. This is now described in some detail.

#### a. Finding the potential

##### 1) HYDROSTATIC POTENTIAL

The hydrostatic pressure field in the interior is obtained by integrating Eq. (20) w.r.t.  $r$  from the (moving)  $r = R_s$  boundary into the interior of the fluid to yield (see Fig. 4):

$$\begin{aligned} \phi &= \phi_s + \int_r^{R_s} -b \, dr \\ &= \phi_s + \int_r^{R_o} -b \, dr + \int_{R_o}^{R_s} -b \, dr \\ &= \phi_s + \int_r^{R_o} -b \, dr + \phi_l, \end{aligned} \quad (40)$$

where  $\phi_l = \int_{R_o}^{R_s} -b \, dr$  is the  $\phi$  at  $r = R_o$  due to the load induced by  $r_s = R_s - R_o$ , Eq. (27).

The boundary condition applied at  $r = R_s$  is

$$\phi_s = \begin{cases} p_s & \text{at ocean surface} \\ gH & \text{at land surface.} \end{cases} \quad (41)$$

Here  $p_s$  is the atmospheric pressure (loading) at the surface of the ocean, see Fig. 3, and  $gH$  is the geopotential height of the orography over land defined by Eq. (34).

##### 2) SURFACE PRESSURE

The surface pressure equation can be obtained by integrating continuity, Eq. (21), vertically from  $r = R_{\text{fixed}}$  to  $r = R_s$

$$\int_{R_{\text{fixed}}}^{R_s} \left( \nabla_r \cdot \mathbf{v}_h + \frac{\partial \dot{r}}{\partial r} \right) dr = 0.$$

Then, applying the kinematic boundary conditions, Eq. (26), we can write

$$\frac{\partial r_s}{\partial t} + \mathbf{v} \cdot \nabla r_s + \int_{R_{\text{fixed}}}^{R_s} \nabla_r \cdot \mathbf{v}_h dr = P_r,$$

where  $r_s = R_s - R_o$  is the free-surface  $r$ -anomaly in units of  $r$ . Using Leibnitz's theorem, the preceding can be rearranged to yield

$$\frac{\partial r_s}{\partial t} + \nabla_h \cdot \int_{R_{\text{fixed}}}^{R_s} \mathbf{v}_h dr = P_r. \quad (42)$$

Equation (42) is stepped forward in time to yield  $r_s$ , which has units of  $r$ —the surface pressure in the atmosphere, the free surface height in the ocean.

Finally we note that in our implementation we approximate  $\Phi_l$  in Eq. (40) by

$$\Phi_l \approx -b_s r_s,$$

where  $b_s$  is the buoyancy at the surface.

#### b. Vertical coordinate and discretization

In our numerical implementation, rather than adopt terrain-following coordinates—for example,  $\sigma$ -coordinates, the standard approach in meteorology [see, e.g., discussions of vertical coordinates in atmospheric models in Simmons and Burridge (1981) and Thuburn (1993)]<sup>5</sup>—we use rescaled height/pressure as a vertical coordinate, as described in Adcroft and Campin (2003). Use of this scaled coordinate ensures that as the vertical resolution of our model is increased, the discrete model mimics the continuous system.

In the atmospheric isomorph, our rescaled pressure

<sup>5</sup> Terrain-following coordinates introduce considerable complications in the ocean because hydrostatic consistency is very difficult to ensure numerically in the presence of steep slopes and islands—see, for example, the discussion in Adcroft et al. (1997).

is the eta coordinate of Mesinger et al. (1988):  $p^* = (p/p_s)p_s^o$ . The coordinate “stretches” with surface pressure variations, as illustrated in Fig. 5 (top). The lower boundary is not a coordinate surface but is fixed in time. Along with this rescaled  $p$ , we employ partial cells to represent topography—as described in Adcroft et al. (1997)—a technique that has considerable advantages over the conventional implementation of eta coordinates.

In the oceanic isomorph we employ  $z^* = [(z - \eta)/(H + \eta)]H$ , as shown in Fig. 5 (bottom). This readily allows one to numerically treat finite-amplitude free-surface effects and the fluxes of  $E - P$  across the sea surface in a physically appealing way.

### 4. Numerical tests of the isomorph hydrodynamical kernel

The experiments described here were carried out using the hydrodynamical kernel described in Marshall et al. (1997a,b) and outlined earlier (see also <http://mitgcm.org>). One model is used in all calculations: isomorphisms are used to render atmospheric and oceanic cousins.

#### a. The atmosphere

The atmospheric isomorph of MITgcm was put through its paces on the cubed sphere, as described in Adcroft et al. (2004), with  $32 \times 32$  grid points per face (C32—nominally  $2.8^\circ$  resolution). The “vector-invariant” form of the momentum equations, on which the model is based, supports any orthogonal curvilinear grid, of which the cubed sphere is a convenient choice permitting uniform gridding and facilitating treatment of polar cap dynamics without the need of a polar filter. The “dry” model is driven by relaxation to a radiative-convective equilibrium profile, following the description set out in Held and Suarez (1994), designed to test

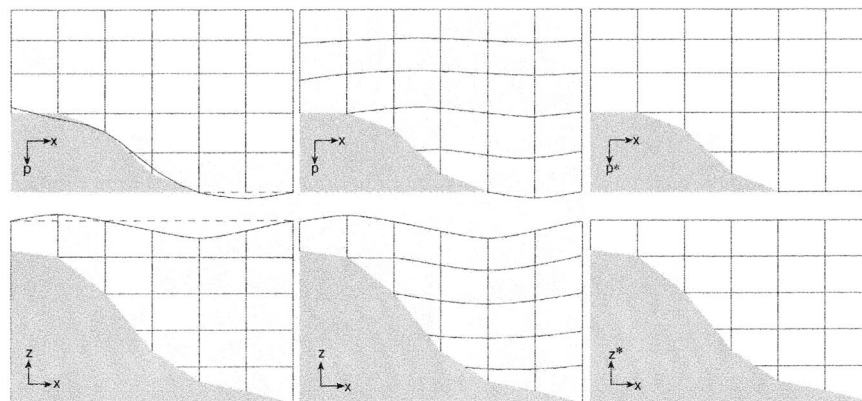


FIG. 5. (top): (right) Rescaled pressure,  $p^*$  follows (middle) surface pressure undulations which are difficult to represent using pressure as (left) a vertical coordinate in atmospheric models. (bottom): (right) Rescaled height,  $z^*$  is designed to follow (middle) free surface undulations which are not readily captured in (left)  $z$ -coordinate ocean models.

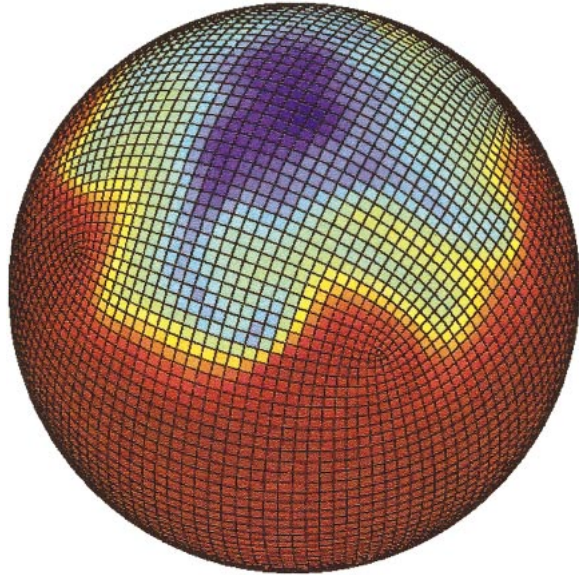


FIG. 6. Instantaneous plot of the temperature field at 500 mb obtained using the atmospheric isomorph of MITgcm on the cubed sphere at C32. The projection of the cube onto the sphere can be clearly discerned in the grid pattern which is also shown.

atmospheric hydrodynamical cores. Twenty equally spaced levels ( $\Delta p = 50$  mb) are used in the vertical. Because of our use of a scaled vertical coordinate, there is no limit to the vertical resolution that can be employed. The forcing and boundary layer friction are specified analytically according to Held and Suarez (1994). As in the finite-difference model described therein, gridpoint noise is controlled using the eighth-order Shapiro (1970) applied to the wind field. Note that in this first example with a flat bottom,  $p^*$  is exactly equivalent to a  $\sigma$  coordinate.

Figure 6 shows an instantaneous plot of the 500 temperature field on the cubed sphere. We see cold air over the pole (blue) and warm air along an equatorial band (red). Fully developed baroclinic eddies spawned in the Northern Hemisphere storm track are evident. Figure 7 shows the 5-yr mean, zonally averaged zonal wind. It compares very favorably with the gridpoint and spectral models described in Held and Suarez (1994). Indeed, on close comparison it is clear that the use of the cubed sphere (obviating the need for polar filters) outperforms the gridpoint model used in Held and Suarez (1994). More detailed comparisons are described in Adcroft et al. (2004).

To further demonstrate how our isomorphed model works in practice we briefly examine the climatology of an atmospheric version of the model (which we call AIM, for atmosphere of intermediate complexity) obtained by “plugging in”—see Fig. 1—the atmospheric package developed by Molteni (2003) into our dynamical core with five vertical levels at C32 on the cubed sphere. Mountains are represented using “partial cells,” as described in Adcroft et al. (1997), with an eta co-

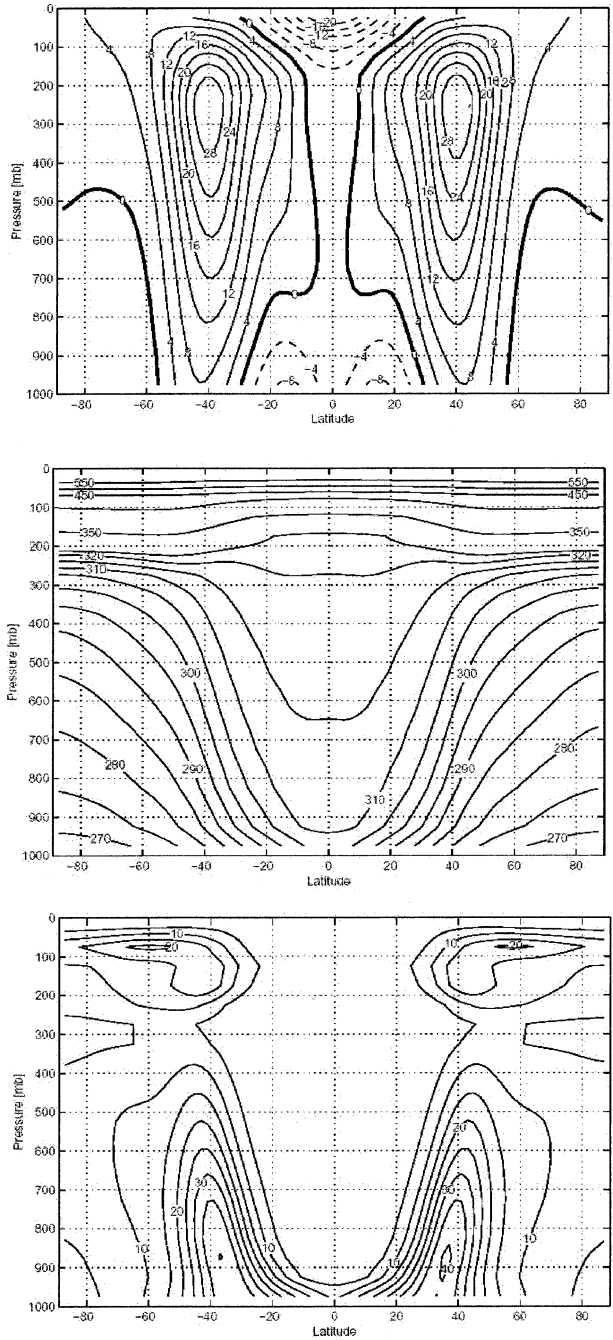


FIG. 7. Zonally averaged (top) zonal flow, (middle) potential temperature, and (bottom) temperature variance from a cube–sphere simulation using Held–Suarez forcing with 20 vertical levels. The solution compares very favorably to that published in Held and Suarez (1994).

ordinate as described in Adcroft and Campin (2003). This example is only presented as a “proof of concept.” The model physics (christened SPEEDY by Molteni (2003) are briefly described in the appendix) are of intermediate complexity and intended to be used in extended coupled climate integrations for studies of pre-

TABLE 1. Parameters used in the ocean circulation experiment.

Horizontal eddy viscosity, $A_h$	$3 \times 10^5 \text{ m}^2 \text{ s}^{-1}$
Vertical eddy viscosity, $A_v$	$1 \times 10^{-3} \text{ m}^2 \text{ s}^{-1}$
Isopycnal/thickness eddy diffusion, $\kappa_{GM}$	$800 \text{ m}^2 \text{ s}^{-1}$
Vertical eddy diffusion, $\kappa_v$	$3 \times 10^{-5} \text{ m}^2 \text{ s}^{-1}$
Enhanced mixing (convection), $\kappa_c$	$10 \text{ m}^2 \text{ s}^{-1}$
Reference density, $\rho_o$	$1035 \text{ kg m}^{-3}$
Level thickness, $\Delta z$ (m)	10, 10, 15, 21, 28, 36, 45, 55, 66, 78, 91, 105, 120, 136, 154, 172, 191, 211, 232, 254, 278, 302, 327, 353, 380, 408, 437, 466, 497, 529

dictability and paleoclimate. Despite the idealized nature of the model “physics” and its crude vertical structure, the model exhibits some realism.

In the experiment described here, AIM is configured with five vertical levels (at 75, 250, 500, 775, and 950 mb)—one in the stratosphere, three in the free troposphere, and one in the planetary boundary layer, as in the model described in Molteni (2003). Monthly mean global sea surface temperature, land temperature, soil moisture, and surface albedo are prescribed. We have compared a wide variety of fields from our isomorphized atmospheric model with that of Molteni (2003)—who coupled SPEEDY physics to the Geophysical Fluid Dynamics Laboratory (GFDL) dynamical core—and find very similar results. Figure 8 compares the zonal average zonal wind with analyzed fields from National Centers for Environmental Prediction (NCEP). There is broad correspondence in the troposphere: the jet streams are of reasonable strength but the trade wind belt is somewhat weak in the troposphere. Modeled anomalies in the height of the 500-mb surface in December–January–February (DJF) are compared with the observations in Fig. 9. The pattern of variability is broadly consistent with observations, but with considerably reduced amplitude. We believe, however, that discrepancies between observed and modeled climatologies are almost entirely a consequence of the highly idealized physics rather than inherent problems with the dynamical core.<sup>6</sup>

### b. Ocean

To illustrate the application of the hydrodynamical kernel configured for the ocean, Figs. 10 and 11 shows a numerical solution on exactly the same cubed grid as the atmospheric model, C32. The model is configured with 15 levels in the vertical with a maximum depth of 5200 m, forced with monthly wind stress (Trenberth et

<sup>6</sup> It should be noted that the vertical coordinate employed in our atmospheric isomorph is not ideally suited to high vertical resolution of, for example, the planetary boundary layer. In this regard, conventional  $\sigma$ -coordinates have a clear advantage over the  $p^*$  coordinate used here. One avenue presently under investigation is to run the “physics” on a different (higher resolution) grid than the dynamics.

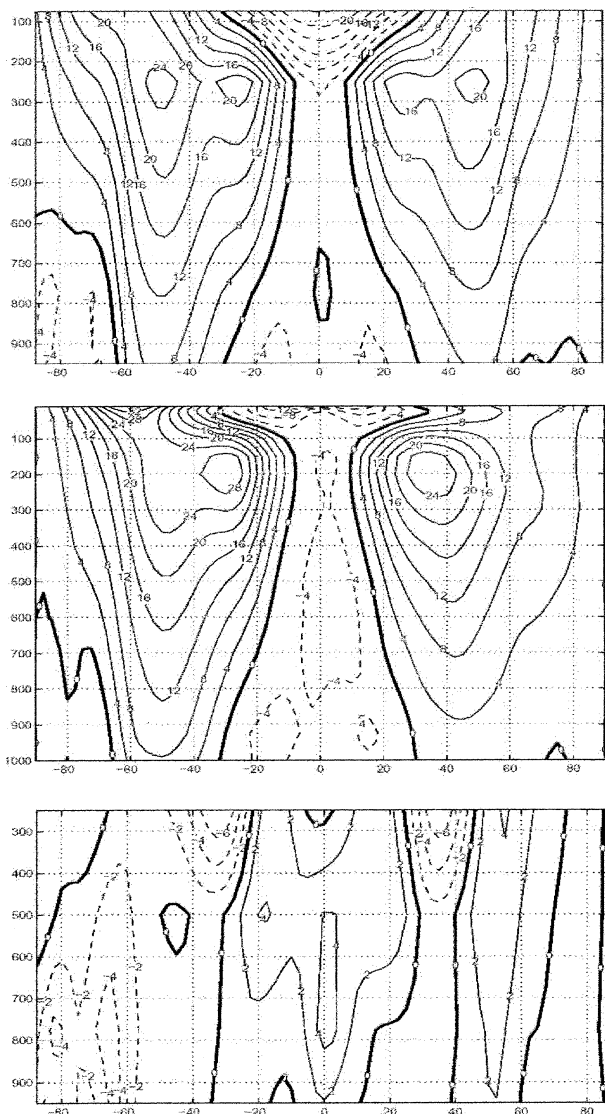


FIG. 8. The zonal-average  $U$  field obtained from (top) a 5-yr integration of the model [contour interval (c.i.) =  $4 \text{ m s}^{-1}$ ] compared to the (middle) NCEP reanalysis (c.i. =  $4 \text{ m s}^{-1}$ ) and (bottom) “model” minus “analysis” (c.i. =  $2 \text{ m s}^{-1}$ ).

al. 1989), monthly observed heat and freshwater fluxes (Jiang et al. 1999), and with a restoring of sea surface temperature and salinity to monthly climatology (Boyer et al. 2002; Stephens et al. 2002). A restoring time scale of two months for SST and two years for salinity is chosen. The model parameters are listed in Table 1. The bathymetry was generated from the Elevation Data for Areas Greater than 50 degrees North (ETOPO5) world bathymetry using a topology-preserving algorithm (A. Adcroft 2002, unpublished manuscript).

Figure 10 shows the streamfunction for the depth-integrated horizontal flow at equilibrium after 5000 yr of integration, revealing the major ocean gyres and the circumpolar current. The global meridional overturning

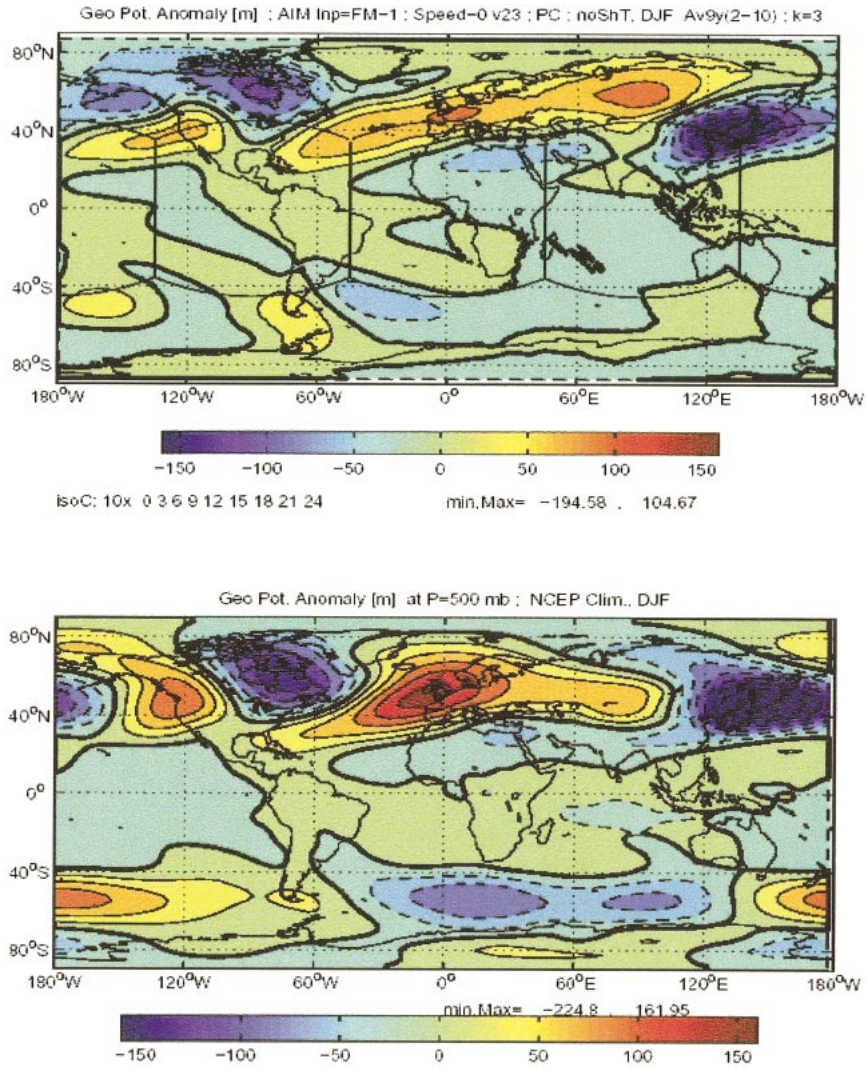


FIG. 9. The geopotential height anomaly of the 500-mb surface in DJF from (top) the AIM model and from (below): the NCEP analysis (c.i. = 30 m).

streamfunction is plotted in Fig. 11 showing downwelling at the northern polar regions and upwelling around Antarctica.

### 5. Conclusions

We have described how mathematical isomorphisms between the equations that govern the atmosphere and ocean can be exploited to design a single hydrodynamical core that can be used to simulate both fluids. Our approach has been illustrated by “plugging in” physics packages to the hydrodynamical core of the MITgcm to render atmospheric and oceanic models of intermediate complexity.

The advantages of the approach outlined here are considerable:

1) Developments of the core hydrodynamics are inher-

ited by both atmosphere and ocean with no extra cost. For example, parallelization of forward hydrodynamics and its differentiation to yield tangent linear and adjoint models—see, for example, Marotzke et al. (1999)—is automatically inherited by both components of the coupled climate system.

2) Models of one fluid could be converted to study the other, by exploiting the isomorphism studied here. Although MITgcm has been designed specifically with the isomorphism in mind, we believe that existing atmospheric<sup>7</sup> (oceanic) cores could, with justifiable effort, be modified to yield an oceanic (atmospheric) counterpart.

<sup>7</sup> The exception would be atmospheric cores based on spectral techniques which cannot be easily modified to describe fluid flow in ocean basins.

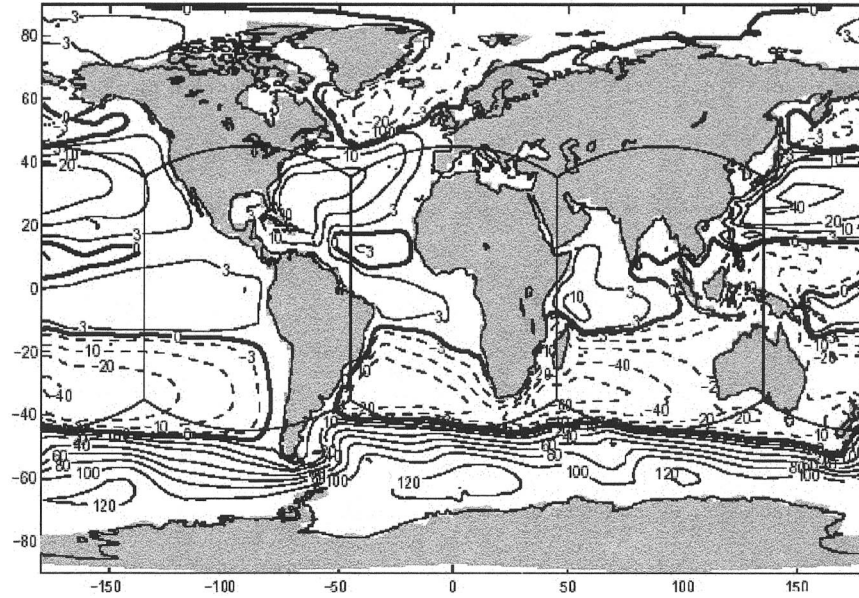


FIG. 10. The streamfunction for the depth-integrated flow obtained from the cubed sphere ocean model. The contour interval is in Sverdrups ( $\text{SV} \equiv 10^6 \text{ m}^3 \text{ s}^{-1}$ ). The edges of the cube are superimposed.

- 3) Coupling of atmospheric and oceanic models is inherently simpler and more logical because the two models can use the same grid. Although in an ideal world the deformation radii of the respective fluids would strongly influence the choice of horizontal resolution, computational economics dictates that, at the present time, horizontal resolutions employed in the two fluids in climate research are roughly comparable ( $\sim 1^\circ$ ). Thus, to our advantage, they can be made equal.
- 4) Working on a common core brings atmospheric and oceanic modelers together and breaks down the artificial barriers between them.

The points just cited are more than “programmatic” issues: the isomorphic approach to the modeling of both fluids advocated here can lead to real innovations. For example, recent examples of model developments driven by applications in one fluid finding immediate application in the other, made possible (and straightforward) by the isomorphism, are

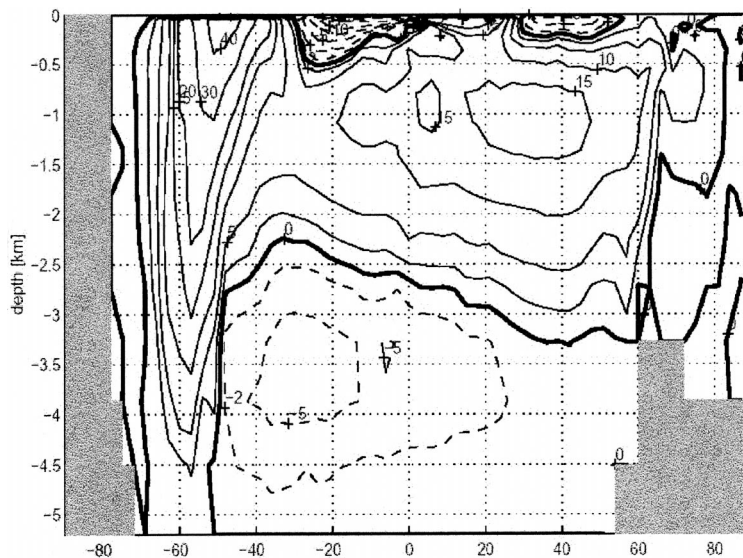


FIG. 11. The global overturning streamfunction (in Sv) obtained from the cubed sphere ocean circulation model.

- 1) The cubed sphere of Adcroft et al. (2004), developed for applications in meteorology, has obvious advantages in the ocean too, with improved treatment of polar cap, ice dynamics, and avoidance of polar filters to lengthen the time step.
- 2) Studies of the importance of the Boussinesq approximation in ocean modeling—as described in de Szoeke and Samelson (2002), non-Boussinesq effects in ocean models can be elegantly taken in to account by adopting pressure as a vertical coordinate. The  $z \leftrightarrow p$  isomorphism outlined here can be readily used to switch between  $z$ -coordinate ocean models and  $p$ -coordinate ocean models—see Losch et al. (2004) where the MITgcm isomorphic kernel is used in this manner.

*Acknowledgments.* This work would not have been possible without support from the ECCO NOPP and MIT's Climate Modeling Initiative.

## APPENDIX

### Details of Model Physics

The distinguishing difference between the atmosphere and the ocean systems is not the dynamics, but rather the source terms that appear on the right-hand sides of Eqs. (1)–(6) and Eqs. (10)–(15) that represent distinct physical processes. To accommodate different physical processes in the two fluids we have constructed component software packages that can be easily switched in and out, as represented schematically in Fig. 1. Substitution of the ocean physics package by an atmospheric physics package is all that is required to transform the model between ocean or atmospheric milieus.

#### a. Atmospheric package

The physics package developed by Molteni (2003) is well suited to exploratory climate simulation and based on the same physical principles as “state-of-the-art” models. It is sufficiently concise that a single person can grasp it in its entirety but, as illustrated in section 4, exhibits considerable realism. Briefly, it utilizes the following limited set of modules parameterizing key processes:

*Surface fluxes of momentum and energy.* Fluxes are defined by bulk aerodynamic formulas with different exchange coefficients between land and sea. Coefficients for (sensible and latent) heat fluxes also depend on the vertical gradient of potential temperature between the surface and the lowest model level.

*Convection.* A simplified mass-flux scheme is activated when conditional instability is present (namely, where saturation moist static energy decreases with height between the planetary boundary layer (PBL) and the two upper-tropospheric layers), and where relative

humidity in the PBL exceeds a fixed threshold. The cloud-base mass flux (at the top of the PBL) is such that the PBL relative humidity is relaxed towards the threshold value. Detrainment occurs only at the cloud-top level (determined by the conditional instability criterion), while entrainment occurs in the lower troposphere if the cloud top is at the highest tropospheric level. The air in the updrafts is assumed to be saturated.

*Large-scale condensation.* When relative humidity exceeds a fixed threshold, specific humidity is relaxed towards the corresponding threshold value, and the latent heat content removed from the atmosphere is converted into dry static energy.

*Cloud cover.* Cloud cover is determined diagnostically from the maximum relative humidity in an air column including all tropospheric layers except the PBL.

*Shortwave radiation.* SW radiation is reflected by clouds at the top of the troposphere and at the surface; the cloud albedo is proportional to the total cloud cover. SW transmissivity is a function of layer mass, specific humidity and cloud cover.

*Longwave radiation.* A four-band LW scheme is used, one for the atmospheric “window” and the others for the absorption by water vapor and carbon dioxide, dependent on the mass and humidity of the layers.

*Vertical diffusion (shallow convection).* Vertical diffusion only acts between the two lowest model layers. Dry static energy and specific humidity are diffused when a conditional instability criterion is satisfied. Otherwise, only humidity is diffused, at a slower rate.

#### b. Ocean package

The oceanic counterparts to the atmospheric physics have been extracted from our core ocean model—see Marshall et al. (1997a,b) and <http://mitgcm.org>. Components that represent ocean-only processes employed in the calculations described here are:

*Convective adjustment.* Statically unstable fluid parcels are homogenized through adjustment or through implicit vertical diffusion.

*Geostrophic eddy parameterization.* Following Gent and McWilliams (1990), tracers are advected by the “Transformed Eulerian Mean” (TEM), expressed as a function of the heat flux by unresolved baroclinic instability, parameterised as a flux down the large-scale temperature gradient. TEM is used together with an along-isopycnal diffusion of tracers.

## REFERENCES

- Adcroft, A. J., and J. M. Campin, 2004: Rescaled height coordinates for accurate representation of free-surface flows in ocean circulation models. *Ocean Modell.*, **7**, 269–284.
- , C. N. Hill, and J. Marshall, 1997: Representation of topography by shaved cells in a height coordinate ocean model. *Mon. Wea. Rev.*, **125**, 2293–2315.
- , J.-M. Campin, C. Hill, and J. Marshall, 2004: Implementation

- of an atmosphere–ocean general circulation model on the expanded spherical cube. *Mon. Wea. Rev.*, **132**, 2845–2863.
- Boyer, T. P., C. Stephens, J. I. Antonov, M. E. Conkright, R. A. Locarnini, T. D. O'Brien, and H. E. Garcia, 2002: *Salinity*. Vol. 2, *World Ocean Atlas 2001*, NOAA Atlas NESDIS 50, 165 pp.
- de Szoeke, R. A., and R. M. Samelson, 2002: The duality between the Boussinesq and Non-Boussinesq hydrostatic equations of motion. *J. Phys. Oceanogr.*, **32**, 2194–2203.
- Eliassen, A., 1949: *The Quasi-static Equations of Motion with Pressure as Independent Variable*. Vol. 17. Geofysiske Publikasjoner, 44 pp.
- Gent, P. R., and J. C. McWilliams, 1990: Isopycnal mixing in ocean circulation models. *J. Phys. Oceanogr.*, **20**, 150–155.
- Haltiner, G., and R. Williams, 1980: *Numerical Prediction and Dynamic Meteorology*. 2d ed. Wiley, 477 pp.
- Held, I. M., and M. J. Suarez, 1994: A proposal for the intercomparison of the dynamical cores of atmospheric general circulation models. *Bull. Amer. Meteor. Soc.*, **75**, 1825–1830.
- Jiang, S., P. Stone, and P. Malanotte-Rizzoli, 1999: An assessment of the GFDL ocean model at coarse resolution: Annual-mean climatology. *J. Geophys. Res.*, **104**, 25 623–25 645.
- Lindzen, R. S., E. S. Batten, and J. W. Kim, 1968: Oscillations in atmospheres with tops. *Mon. Wea. Rev.*, **96**, 133–140.
- Losch, M., A. Adcroft, and J.-M. Campin, 2004: How sensitive are coarse general circulation models to fundamental approximations in the equations of motion? *J. Phys. Oceanogr.*, **34**, 306–319.
- Marotzke, J., R. Giering, K. Q. Zhang, D. Stammer, C. Hill, and T. Lee, 1999: Construction of the adjoint MIT ocean general circulation model and application to Atlantic heat transport variability. *J. Geophys. Res.*, **104** (C12), 29 529–29 547.
- Marshall, J., A. Adcroft, C. Hill, L. Perelman, and C. Heisey, 1997a: A finite-volume, incompressible Navier Stokes model for studies of the ocean on parallel computers. *J. Geophys. Res.*, **102** (C3), 5753–5766.
- , C. Hill, L. Perelman, and A. Adcroft, 1997b: Hydrostatic, quasi-hydrostatic, and nonhydrostatic ocean modeling. *J. Geophys. Res.*, **102** (C3), 5733–5752.
- Mesinger, F., Z. I. Janjić, S. Ničković, D. Gavrilov, and D. G. Deaven, 1988: The step-mountain coordinate: Model description and performance for cases of Alpine lee cyclogenesis and for a case of Appalachian redevelopment. *Mon. Wea. Rev.*, **116**, 1493–1518.
- Molteni, F., 2003: Atmospheric simulations using a GCM with simplified physical parameterizations. I: Model climatology and variability in multi-decadal experiments. *Climate Dyn.*, **20** (2–3), 175–191.
- Phillips, N. A., 1957: A coordinate system having some special advantages for numerical forecasting. *J. Meteor.*, **14**, 184–185.
- Shapiro, R., 1970: Smoothing, filtering and boundary effects. *Rev. Geophys. Space Phys.*, **8**, 359–387.
- Simmons, A. J., and D. M. Burridge, 1981: An energy and angular-momentum conserving vertical finite difference scheme and hybrid vertical coordinates. *Mon. Wea. Rev.*, **109**, 758–766.
- Stephens, C., J. I. Antonov, T. P. Boyer, M. E. Conkright, R. A. Locarnini, T. D. O'Brien, and H. E. Garcia, 2002: *Temperature*. Vol. 1, *World Ocean Atlas 2001*, NOAA Atlas NESDIS 49, 167 pp.
- Thuburn, J., 1993: Baroclinic-wave life cycles, climate simulations and cross-isentrope mass flow in a hybrid isentropic coordinate GCM. *Quart. J. Roy. Meteor. Soc.*, **119**, 489–508.
- Trenberth, K., J. Olson, and W. Large, 1989: A global ocean wind-stress climatology based on ECMWF analyses. NCAR Tech. Rep. NCAR/TN-338+STR, Boulder, CO, 105 pp.